Unmanned Aerial Remote Sensing System (UARSS)-Derived Normalized Difference Vegetation Index (NDVI) to Soil Moisture Mapping

Tung-Ching Su, National Quemoy University, Taiwan

The Asian Conference on Sustainability, Energy & the Environment 2017
Official Conference Proceedings

Abstract
While satellite remote sensing systems have been widely applied to soil moisture monitoring, they are unsuitable for soil moisture monitoring of small areas, which merely cover several hectares, due to their low spatial or temporal resolutions. In order to address this problem, a multispectral sensor, Parrot Sequoia, carried on an unmanned aerial vehicle (UAV) is adopted to acquire the multispectral images with green (0.550 μm), red (0.660 μm), red-edge (0.735μm), and near-infrared (0.790 μm) bands, as well as the geometric resolution of 0.2 m. Thus, thematic maps of Normalized Difference Vegetation Index (NDVI) can be derived by the differentiation of spectral responses between red and either red-edge or near-infrared. In this research, an agricultural field in Kinmen, Taiwan was selected as the study site, and several *in situ* sampling points were schemed for monthly data acquisition of soil moisture at two depths: 10 cm and 20 cm. Based on the *in situ* sampling data and the thematic maps of NDVI, an empirical model was established for soil moisture mapping. The preliminary results show that NDVI offers a good explanation for soil moisture at deep depth. The range of the estimated soil moistures are approximately between 10 and 20%.

Keywords: Unmanned Aerial Vehicle (UAV), Multispectral Sensor, Normalized Difference Vegetation Index (NDVI), Soil Moisture, Empirical Model

1. Introduction

Soil moisture monitoring, which is usually implemented by the satellite-based remote sensing techniques (Wang, et al., 2007; Chen, et al., 2014; Mladenova, et al., 2014; Petropoulos, et al., 2015), has also been widely applied to hazard prevention (Hawke & McConchie, 2011; Laiolo, et al., 2016), agricultural management (Mallick, et al., 2009; Sakai, et al., 2016), and climate (Schnur, et al., 2010; Dente, et al., 2012; Fang, et al., 2016). Based on the satellite images, Wang, et al. (2007) and Chen, et al. (2014) calculated the normalized difference of vegetation indices (NDVIs) to establish the correlations between the NDVIs and soil moisture. Mladenova, et al. (2014) reviewed the passive microwave-based techniques and the soil moisture retrieval algorithms, where NDVI is involved. The spatial resolution of satellite images, such as the 250 m/pixel of Moderate Resolution Imaging Spectroradiometer (MODIS), is capable of NDVI analysis of country or continental scales, but is unsuitable for small areas merely covering several hectares. Furthermore, Wang, et al. (2007) and Petropoulos, et al. (2015) both indicated that while passive microwave radiometry and active microwave radar, such as synthetic aperture radar (SAR), have been widely applied to soil moisture mapping, the radar signal only penetrates soil surface to several centimeters so that only the soil moisture of the top few centimeters can be mapped. In this research, an unmanned aerial vehicle (UAV) due to its flexibility as well as reliability is considered as a good vehicle to carry a multispectral sensor for the acquisition of remote sensing data with high spatial resolution.

Currently, there are many applications of unmanned aerial remote sensing systems (UARSSs) to water quality monitoring (Su & Chou, 2015; Su, 2017; Guimarães, et al., 2017), forestry (Zarco-Tejada, et al., 2014; Chianucci, et al., 2016), agriculture (Bendig, et al., 2015; Gago, et al., 2015; Santesteban, et al., 2017; Romero-Trigueros, et al., 2017), and disaster management (Niethammer, et al., 2012). In particular, Bendig, et al. (2015) indicated that NDVI is useful for biomass monitoring of barley, and shows positive correlation related to water stress for agriculture (Gago, et al., 2015). Based on the above reviews, a linear regression model between calculated NDVI and observed soil moisture is established for soil moisture mapping. Additionally, a correlation between precipitation and soil moisture is also discussed in this paper.

2. Study Site and Soil Moisture Examination

Figure 1 shows the true color image of the study site, which covers approximately 100,000 m^2. In the study site, the land use includes agriculture, forest, water body, and path. On January 15, 2017, February 15, 2017, April 8, 2017, and May 4, 2017, at a total of twelve sampling points soil moisture was examined at two depths: 10 and 20 cm. The examination results are shown in Table 1.

Wang, et al. (2007) investigated the influence of soil moisture at different depths on NDVI and indicated that NDVI has a strong correlation with the water stress of vegetation. NDVI is also related to ground temperature varying with precipitation (Schnur, et al., 2010). At present, Table 1 cannot show a significant correlation between depth and soil moisture, but along with the accumulated sampling points, the correlation is still worth future discussion.

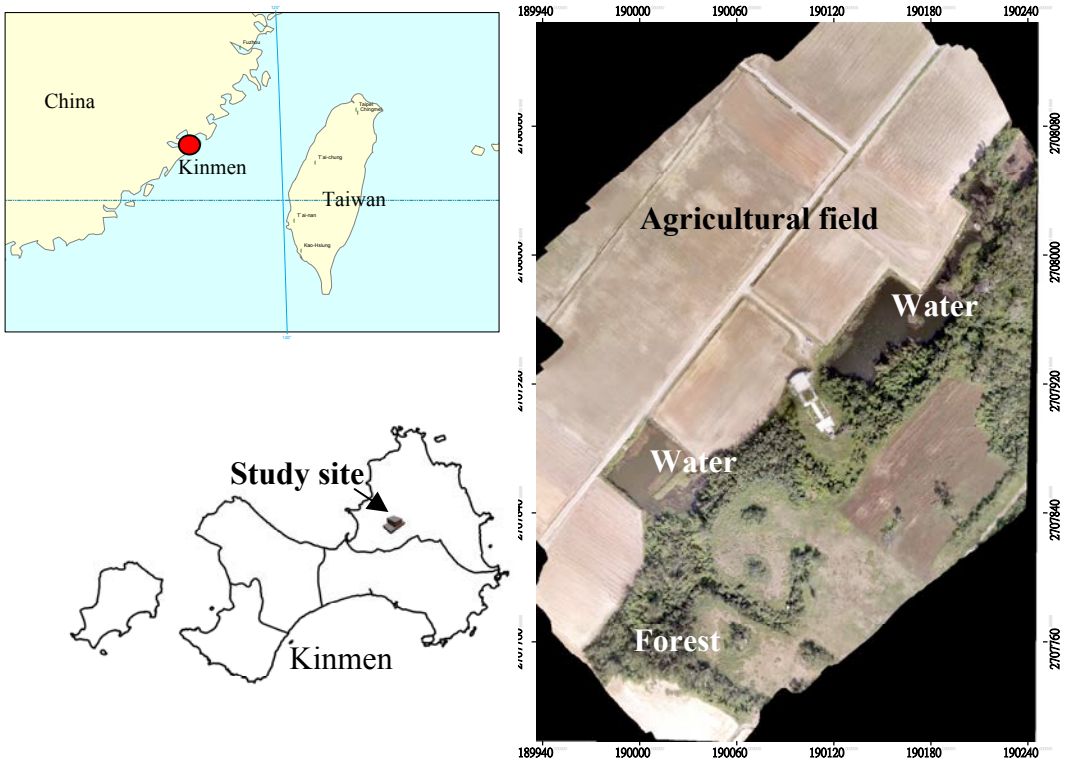

Figure 1: True color image of study site.

3. Unmanned Aerial Remote Sensing System (UARSS)

3.1 Unmanned Aerial Vehicle (UAV) and Flying Control System

A UAV with four rotor wings was chosen to carry the multispectral sensor (see Figure 2). The technical features of the UARSS include four 1.2 mega pixels sensors (near-infrared (NIR), red-edge (RE), red (R), and green (G)), as well as one 16 mega pixels RGB sensor (see Figure 3), ground resolution at 190 m of 0.2 cm/pixel, distance between two flying strips of approximately 65 m, image pitch of 256 × 192 m^2, and end and side laps of 80% and 70%, respectively. The weather conditions, including visibility of 7000 m and cloud level of 3000 m, are also required.

Figure 4 shows an interface of the flying control system. Orientation, height, speed, and camera station can be instantaneously displayed on the interface, so global position system (GPS) and inertial measurement unit (IMU) are the two critical devices in the UARSS. Before implementing a flight task, the schemed flying strips must be input into the flying control system. During the flight task, the UAV can be precisely directed forward along the schemed flying strips, and the flying control system can automatically press the shutters at the correct camera stations (see Figure 5).

3.2 Multispectral Sensor and Image Data

For a unique scene, the multispectral sensor, shown as Figure 3, can offer four gray-level images in the channels, i.e. G (0.550 μm), R (0.660 μm), RE (0.735μm), and NIR (0.790 μm), and a RGB image. Both of the RE and NIR channels belong to the invisible spectrums. RE is a narrow channel between R and NIR, so RE is effective in

discriminating vegetation against non-vegetation. The study site was imaged on December 8, 2016, February 17, 2017, April 7, 2017, and May 5, 2017. Figure 6 shows the multi-temporal false color images of the study site. Because the multispectral sensor has the RE and NIR channels, two kinds of false color images can be obtained.

Table 1: Soil moisture examination of sampling *in situ*.

Sampling date	Coordinate system: GCS_TWD_1997			Depth (cm)	Soil moisture (%)
	ID	N	E		
January 15, 2017	1	2707927	190091	10	11.86
				20	13.57
	2	2707927	190089	10	21.73
				20	18.17
	3	2707906	190111	10	5.36
				20	5.30
February 15, 2017	4	2707946	190093	10	13.17
				20	14.92
	5	2707904	190113	10	3.45
				20	3.35
April 8, 2017	6	2708014	190084	10	6.48
				20	7.28
	7	2707967	189996	10	18.89
				20	17.91
	8	2707968	190064	10	13.25
				20	32.12
May 4, 2017	9	2707947	190091	10	17.19
				20	12.51
	10	2707952	190047	10	12.91
				20	11.81
	11	2707999	190046	10	11.97
				20	14.56
	12	2708011	190074	10	11.67
				20	14.98

4. Methodology

4.1 Calculation of NDVI

In each monitoring task, the study site will obtain two false color images (see Figure 6). Thus, the following two NDVIs are presented in this paper:

$$NDVI\_1 = (NIR - R) / (NIR + R), \quad (1)$$

$$NDVI\_2 = (RE - R) / (RE + R). \quad (2)$$

NDVI being equal to 1 means that the R channel has no spectral response; on the contrary, if either the NIR or RE channel has no spectral response, NDVI is equal to -1. Thus, NDVI ranges between -1 (not good vegetation) and 1 (good vegetation).

Figure 2: UAV with four rotor wings.

Figure 3: Multispectral sensor.

Figure 4: Flying control system.

Figure 5: Flying strips and camera stations.

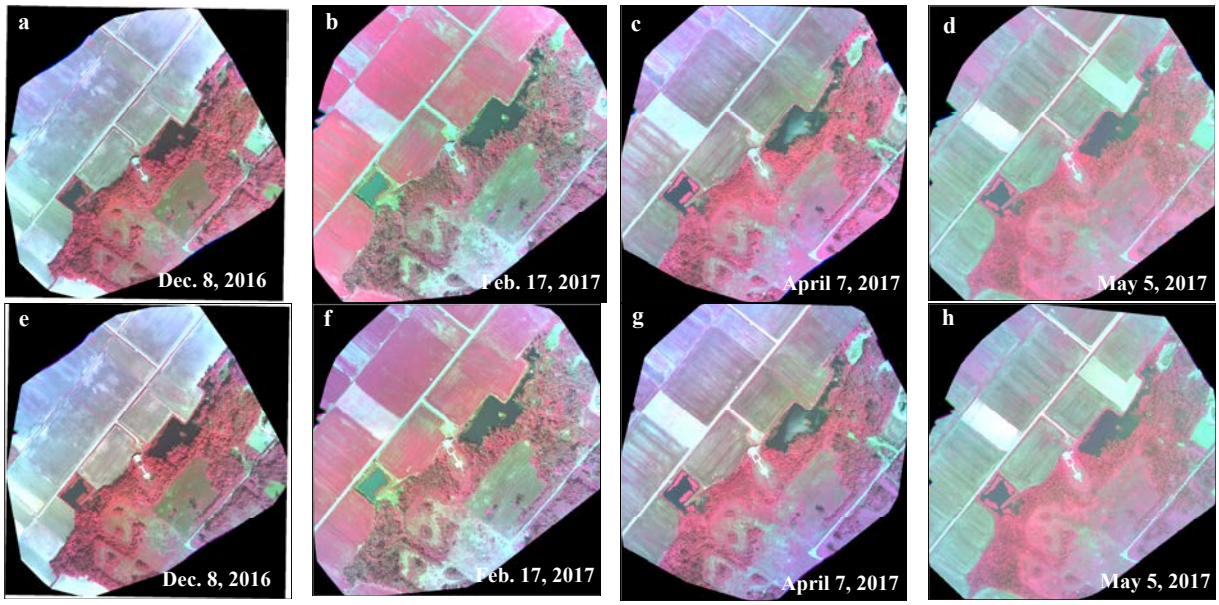

Figure 6: False color images of the study site; (a) through (d) Images consisting of channel 1: NIR, channel 2: R, and channel 3: G; (e) through (h) Images consisting of channel 1: RE, channel 2: R, and channel 3: G.

4.2 Empirical model

Vegetation status usually is related to soil moisture of the root zone (Alvarez-Garreton, et al., 2015; Laiolo, et al., 2016); precipitation-runoff and land uses also influence soil the moisture of the root-zone (Renzullo, et al., 2014). In this research, a

linear regression model between NDVI and soil moisture is introduced. Referring to the linear model of Wang, et al. (2007), the empirical model for soil moisture mapping is represented as:

$$\mathbf{Y} = a \cdot \mathbf{X} + b, \tag{3}$$

$$a = (\mathbf{X}'\mathbf{X})^{-1}\mathbf{X}'\mathbf{Y}, \tag{4}$$

$$\acute{\mathbf{Y}} = \mathbf{X} \cdot a, \tag{5}$$

where **X**, **Y,** a, and b signify NDVI, soil moisture, constant, and random error, respectively. Estimated soil moisture ($\acute{\mathbf{Y}}$) can be explained by NDVI (**X**) according to a square of Pearson correlation coefficient.

5. Preliminary Results and Discussion

5.1 NDVI calculation

Based on the false color images in Figure 6, the NDVIs of the study site are calculated and shown as Figure 7. The statistics of the NDVIs in Figure 7 are shown as the histograms in Figure 8. Compared with the statistical histograms of NDVI_1 and NDVI_2, the statistical histograms have similar patterns and the approximate NDVI ranges. The NDVI ranges in late 2016 and early 2017 both were -0.4 ~ 0.4. Based on NDVI_1, the standard deviation for the statistical histograms in the period of December 2016 through April 2017 was slightly increased from 0.026 to 0.039 but reduced to 0.027 in May 2017. Based on NDVI_2, however, there is a steady standard deviation of approximately 0.027 for the statistical histograms in the period of December 2016 through May 2017. The above result demonstrates that the NIR and RE channels have similar performance in NDVI calculation. Moreover, NDVI_1 has the better capacity than NDVI_2 for detecting slight difference of vegetation biomass.

Due to the growth of the wheat, the gray levels of the agricultural field in early 2017 are obviously brighter than those in late 2016 (see Figure 7). However, the forest had darker gray levels in early 2017 than in late 2016. Compared with Figures 8(a) and (b), there is the more number of pixels with the NDVIs between 0.2 and 0.4 in early 2017 than in late 2016. This result demonstrates that the growth of the wheat leaded to an increase of the number of pixels with the above positive NDVIs. On the contrary, a decrease of the forest biomass resulted in the increase of the number of pixels with the negative NDVIs between -0.2 and -0.4. After April 2017, the wheat was reaped so that the agricultural field displayed bare soil. Figures 8(b) through (d) are seen that the number of pixels with the positive NDVIs after April 2017 is significantly less than in February 2017.

Figure 9 shows the monthly precipitation from November 2016 to May 2017; it can be conjectured that the darker gray levels of the forest in early 2017 are related to the precipitation. The monthly precipitation suddenly dropped from 123.1mm in November 2016 to 28mm in December 2016. Whereas the precipitation in February 2017 is greatly increased, the growth of the forest is healthier after than before February 2017. Thus, the soil moisture of the forest also should be increased after February 2017. Theoretically an increased precipitation will induce an increase of

vegetation biomass to raise NDVIs, but the vegetation biomass in the agricultural field is additionally controlled by farming that hampers this study to establish a robust correlation between NDVI and soil moisture.

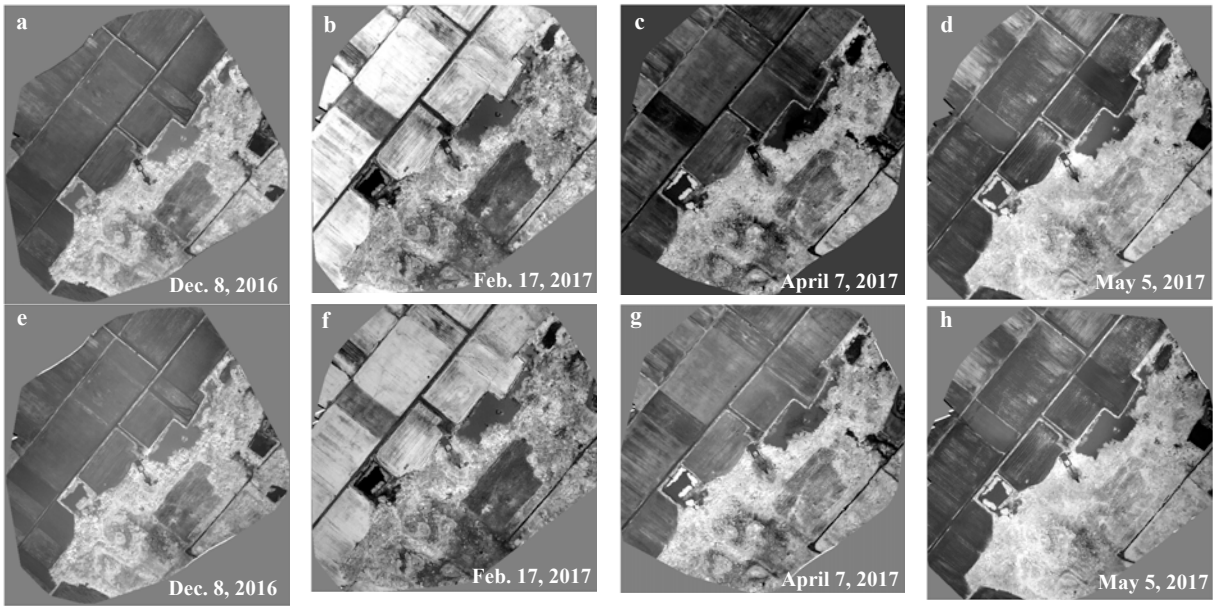

Figure 7: NDVI calculation results; (a) through (d) NDVI_1; (e) through (h) NDVI_2.

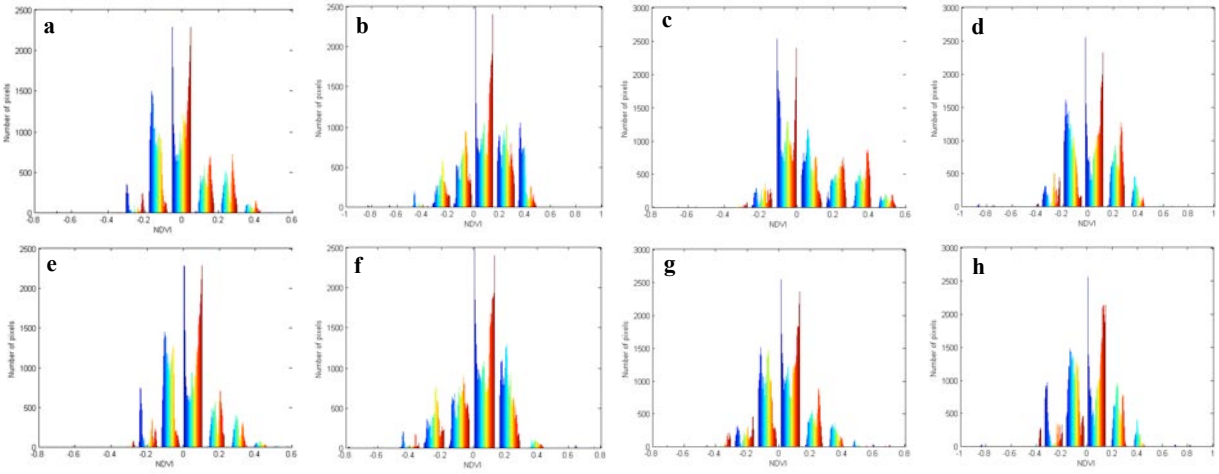

Figure 8: Statistical histograms corresponding to Figure 7.

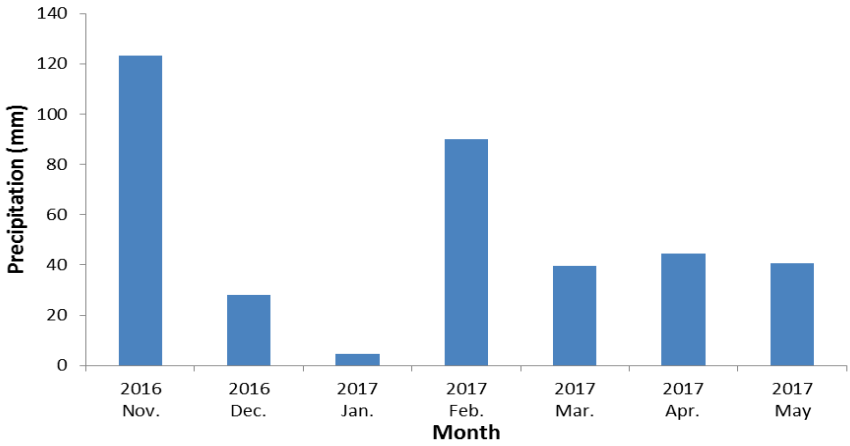

Figure 9: Monthly precipitation.

Table 2: NDVI calculation results of *in situ* sampling points.

Date of UARSS imaging	ID of sampling *in situ*	NDVI_1	NDVI_2
December 8, 2016	1	-0.1173	-0.0642
	2	-0.1256	-0.0601
	3	-0.0017	0.0059
February 17, 2017	4	-0.3132	-0.2414
	5	-0.0373	-0.0049
April 7, 2017	6	-0.0513	-0.0289
	7	-0.1099	-0.0940
	8	0.0794	0.0749
May 5, 2017	9	0.1730	0.1610
	10	0.0203	0.0298
	11	0.0306	0.0364
	12	-0.1232	-0.1072

5.2 Empirical Model Establishment

Table 2 lists the NDVI calculation results for the *in situ* sampling points. Based on Tables 1 and 2, the empirical models' correlations between NDVI and soil moisture are established, as shown in Figure 10. So far there is not a significant correlation between the NDVIs and the soil moisture. Nevertheless, Figures 10(a) and (c) show the negative correlation between NDVI and soil moisture that is contrary to the expected positive correlation. It is evident that some of the sampling points, i.e. the IDs of 1 through 3, have a temporal gap of approximately one month between the UARSS imaging and the measurement *in situ*. Theoretically, a higher NDVI should reflect higher soil moisture strengthening vegetation biomass, but the correlation between NDVI and soil moisture is negative; this may result from the temporal gap or the positioning precision limit of 5 m of our handheld GPS. Considering the positioning precision limit, an NDVI in Table 2 is derived by averaging the NDVIs in an area of 5×5 m^2. In the averaged NDVI, the NDVIs of land uses of non-vegetation, such as bare soil, are also probably involved, so in Table 2 some of the averaged NDVIs are negative. In spite of that, currently the sampling size of soil moisture examination is too small to identify the precise correlation between NDVI and soil moisture. Long-term monitoring of soil moisture is still needed in this research.

Due to the negative correlations in Figures 10(a) and (c), the observed soil moistures at the shallow depth cannot be reasonably explained by the calculated NDVIs. The obtained empirical models in Figures 10(a) and (c) are abandoned in the next stage of soil moisture mapping. Between Figures 10(b) and (d), NDVI_2 compared to NDVI_1 has the better explanation for the observed soil moistures at the deep depth. In other words, the RE channel, where the channel width is about 0.01 μm, is more useful than the NIR channel, where the channel width is about 0.03~0.04 μm, in the establishment of the empirical model. Also, the RE channel should be more sensitive than the NIR one in soil moisture detection.

5.3 Soil Moisture Mapping

According to the linear models shown as Figures 10(b) and (d), the mapping results for the soil moistures at the depth of 20 cm are shown as Figures 11 and 12.

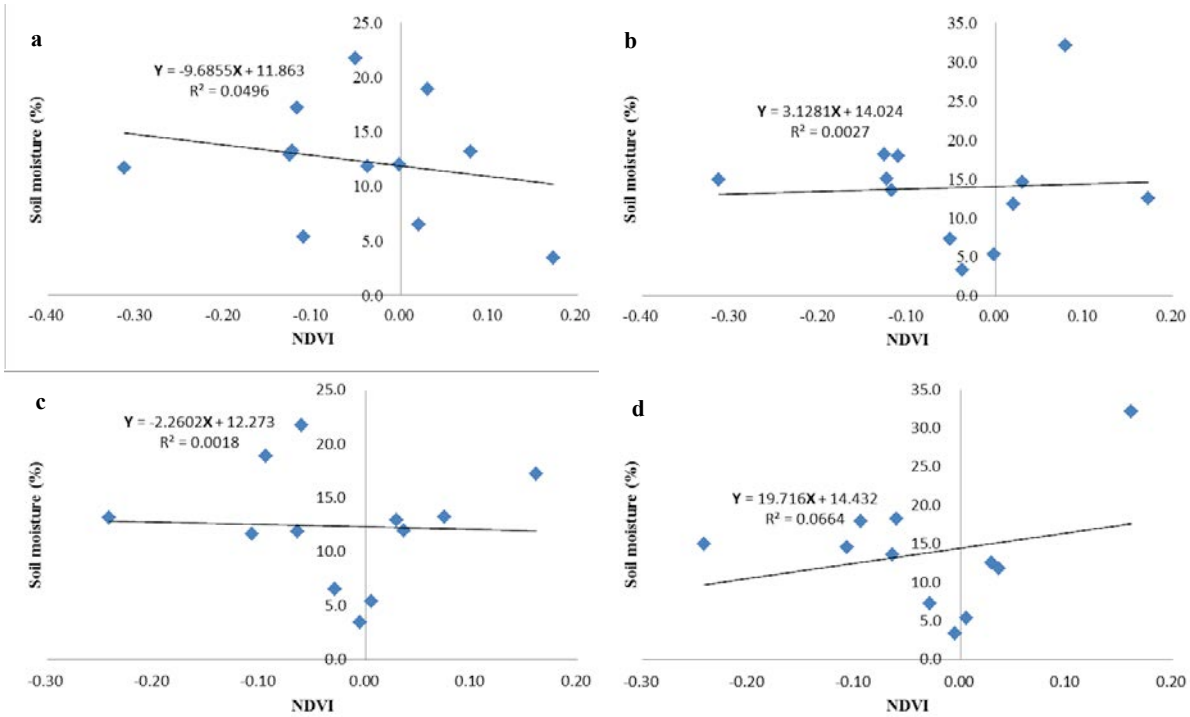

Figure 10: Empirical models; (a) and (b) show the models between NDVI_1 and soil moisture at the depths of 10 and 20 centimeters, respectively; (c) and (d) show the models between NDVI_2 and soil moisture at the depths of 10 and 20 centimeters, respectively.

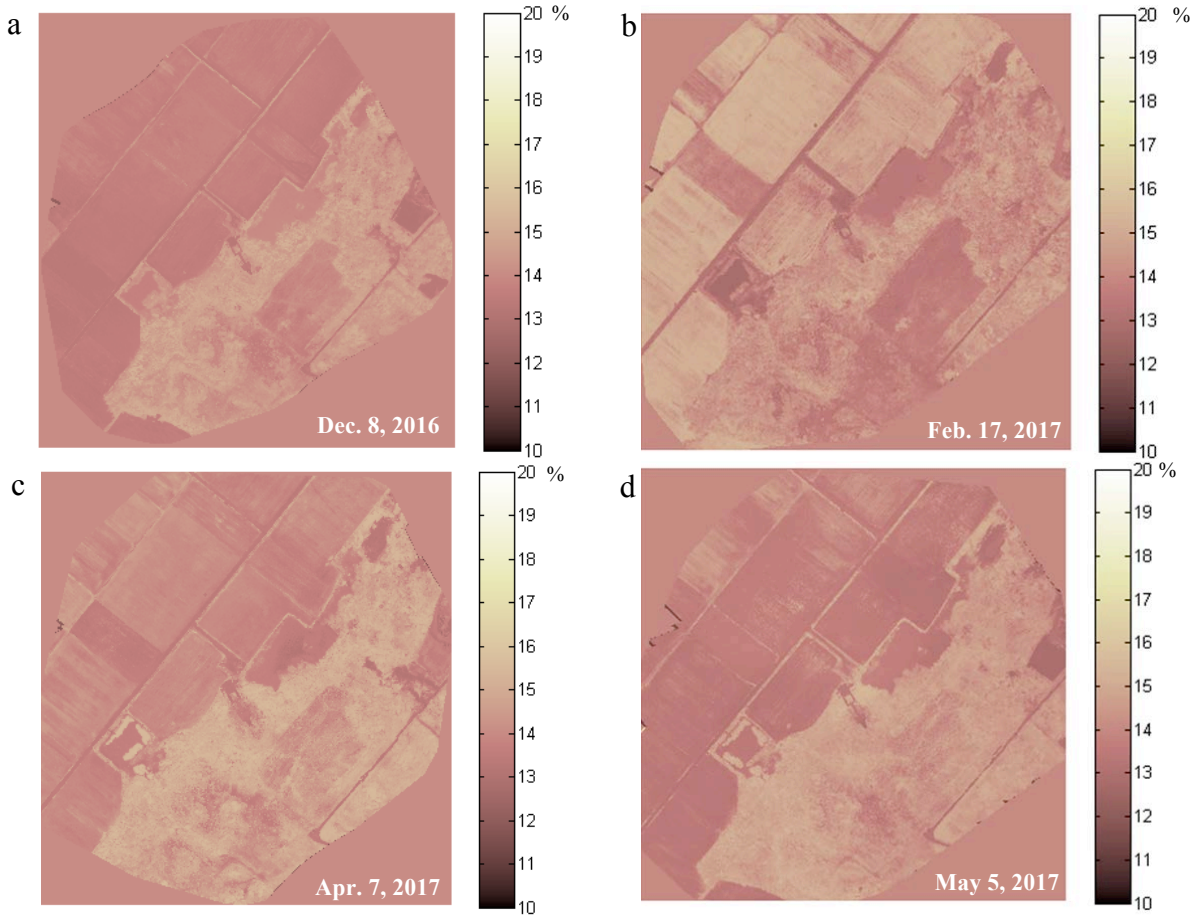

Figure 11: Using the empirical model of **Y** = 3.1281**X** + 14.024 for soil moisture mapping at the depth of 20 cm.

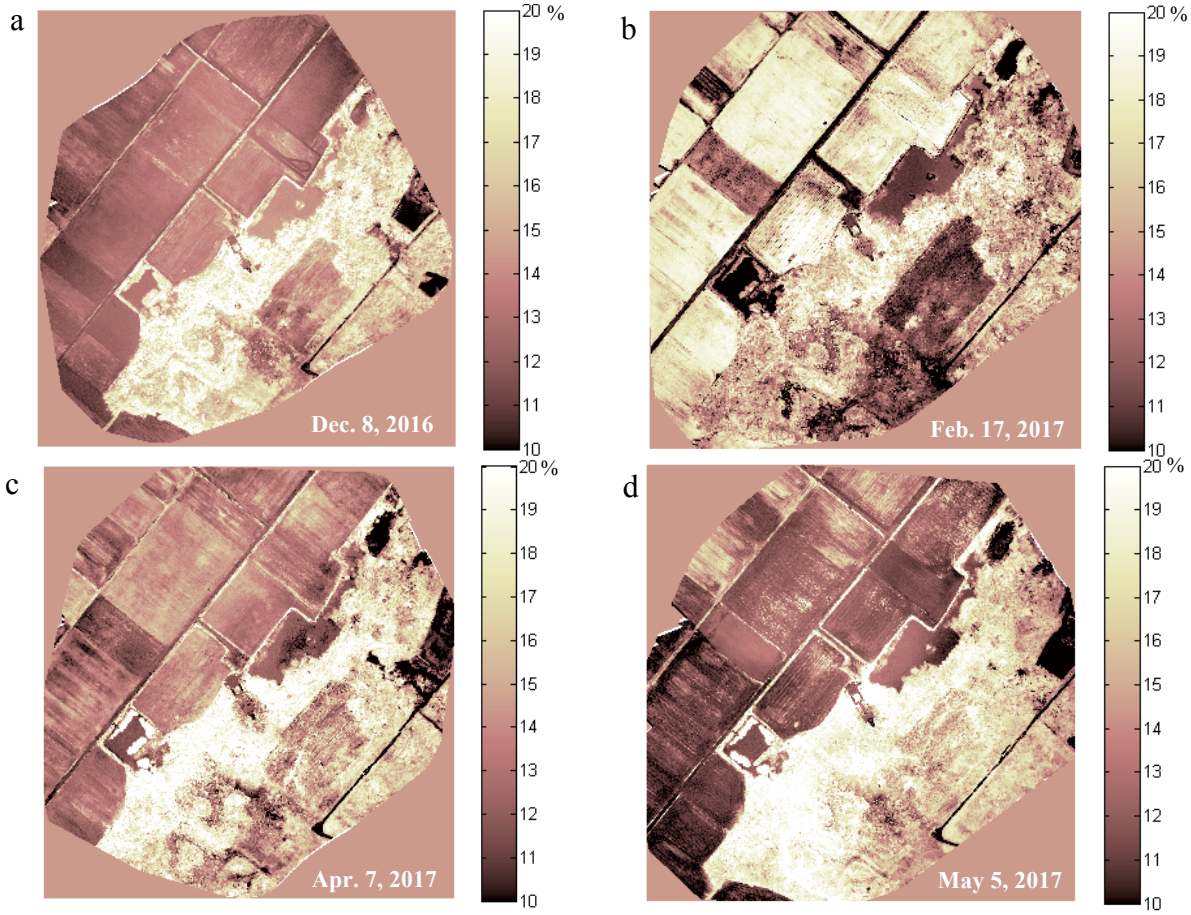

Figure 12: Using the empirical model of **Y** = 19.716**X** + 14.432 for soil moisture mapping at the depth of 20 cm.

The soil moisture mapping in Figure 11 is produced by the empirical model of **Y** = 3.1281**X** + 14.024. In December 2016, the estimated soil moistures in the agricultural field are approximately between 13 and 14%. Along with the growth of the wheat, the soil moistures mostly between 15 and 16% are estimated for the agricultural field in February 2017. In April or May 2017, the estimated soil moistures in the agricultural field drop back between 13 and 14%. However, the drop of the estimated soil moistures results from the radiometric reflectance decrease of the NIR channel due to the reaped wheat. The estimation precision for the agricultural field still needs to be surveyed in the future. As for the forest, the variation of the estimated soil moistures is just contrary to that of the agricultural field. In December 2016, the estimated soil moistures in the forest are approximately between 14 and 15%. Along with the decrease of the precipitation, the estimated soil moistures are also slightly decreased in February 2017. In April or May 2017, the estimated soil moistures in the forest approximately reach to 15%.

The variation tendency of the estimated soil moistures in Figure 12 is similar to that in Figure 11. Nevertheless, the soil moisture mapping has the better contrast in Figure 12 than in Figure 11 because the RE channel should be more sensitive than the NIR one in soil moisture detection. In conclusion the above results of soil moisture mapping

demonstrate that climate factor, such as precipitation, could influence soil moisture. However, human activity, such as farming, would hamper soil moisture estimation.

6. Conclusion

This paper presents a UARSS technique and discusses the influences of precipitation, soil depth, and invisible channels on soil moisture mapping. The UARSS demonstrated its potential for establishing the correlation between precipitation and soil moisture. The current size of sampling *in situ,* and the remote sensing data are still insufficient, but some preliminary results have been obtained in this paper. Firstly, NDVI is calculated based on the spectral channels of R, RE, and NIR of Parrot Sequoia, and demonstrated its effectiveness in soil moisture mapping. Moreover, RE compared with NIR can establish a better empirical model between NDVI and soil moisture. Secondly, precipitation and human activity both would impact soil moisture, and NDVI offers a good explanation for soil moisture at deep depth. At present, the obtained correlation between NDVI and soil moisture at shallow depth is negative, which is contrary to the hypothesis of positive correlation. In the future, the correlation between NDVI and soil moisture still needs to be correctly identified, and an estimation accuracy of soil moisture mapping also needs to be surveyed.

Acknowledgements

This research was performed within the framework of the project “A research of risk classification, performance assessment, monitoring and management for historical sites in Kinmen ─Environmental issue”, as funded by the Ministry of Science and Technology, Taiwan (MOST 105-2410-H-507 -002 -).

References

Alvarez-Garreton, C., Ryu, D., Western, A. W., Su, C.-H., Crow, W. T., Robertson, D. E., & Leahy, C. (2015). Improving operational flood ensemble prediction by the assimilation of satellite soil moisture: comparison between lumped and semi-distributed schemes. *Hydrology and Earth System Sciences, 19, 1659–1676*.

Bendig, J., Yu, K., Aasen, H., Bolten, A., Bennertz, S., Broscheit, J., Gnyp, M. L., & Bareth, G. (2015). Combining UAV-based plant height from crop surface models, visible, and near infrared vegetation indices for biomass monitoring in barley. *International Journal of Applied Earth Observation and Geoinformation, 39, 79–87*.

Chen, T., de Jeu, R. A. M., Liu, Y. Y., van der Werf, G. R., & Dolman, A. J. (2014). Using satellite based soil moisture to quantify the water driven variability in NDVI: A case study over mainland Australia. *Remote Sensing of Environment, 140, 330–338*.

Chianucci, F., Disperati, L., Guzzi, D., Bianchini, D., Nardino, V., Lastri, C., Rindinella, A., & Corona, P. (2016). Estimation of canopy attributes in beech forests using true colour digital images from a small fixed-wing UAV. *International Journal of Applied Earth Observation and Geoinformation, 47, 60–68*.

Dente, L., Vekerdy, Z., Wen, J., & Su, Z. (2012). Maqu network for validation of satellite-derived soil moisture products. *International Journal of Applied Earth Observation and Geoinformation, 17, 55–65*.

Fang, L., Hain, C. R., Zhan, X., & Anderson, M. C. (2016). An inter-comparison of soil moisture data products from satellite remote sensing and a land surface model. *International Journal of Applied Earth Observation and Geoinformation, 48, 37–50*.

Gago, J., Douthe, C., Coopman, R. E., Gallego, P. P., Ribas-Carbo, M., Flexas, J., Escalona, J., & Medrano, H. (2015). UAVs challenge to assess water stress for sustainable agriculture. *Agricultural Water Management, 153, 9–19*.

Guimarães, T. T., Veronez, M. R., Koste, E. C., Gonzaga Jr., L., Bordin, F., Inocencio, L. C., Larocca, A. P. C., de Oliveira, M. Z., Vitti, D. C., & Mauad, F. F. (2017). An alternative method of spatial autocorrelation for chlorophyll detection in water bodies using remote sensing. *Sustainability, 9, 416*.

Hawke, R., & McConchie, J. (2011). In situ measurement of soil moisture and pore-water pressures in an 'incipient' landslide: Lake Tutira, New Zealand. *Journal of Environmental Management, 92*, *266–274*.

Laiolo, P., Gabellani, S., Campo, L., Silvestro, F., Delogu, F., Rudari, R., Pulvirenti, L., Boni, G., Fascetti, F., Pierdicca, N., Crapolicchio, R., Hasenauer, S., & Puca, S. (2016). Impact of different satellite soil moisture products on the predictions of a continuous distributed hydrological model. *International Journal of Applied Earth Observation and Geoinformation, 48, 131–145*.

Mallick, K., Bhattacharya, B. K., & Patel, N. K. (2009). Estimating volumetric surface moisture content for cropped soils using a soil wetness index based on surface temperature and NDVI. *Agricultural and Forest Meteorology, 149, 1327–1342*.

Mladenova, I. E., Jackson, T. J., Njoku, E., Bindlish, R., Chan, S., Cosh, M. H., Holmes, T. R. H., de Jeu, R. A. M., Jones, L., Kimball, J., Paloscia, S., & Santi, E. (2014). Remote monitoring of soil moisture using passive microwave-based techniques — Theoretical basis and overview of selected algorithms for AMSR-E. *Remote Sensing of Environment, 144, 197–213*.

Niethammer, U., James, M. R., Rothmund, S., Travelletti, J., & Joswig, M. (2012). UAV-based remote sensing of the Super-Sauze landslide: Evaluation and results. *Engineering Geology, 128, 2–11*.

Petropoulos, G. P., Ireland, G., & Barrett, B. (2015). Surface soil moisture retrievals from remote sensing: Current status, products & future trends. *Physics and Chemistry of the Earth, 83–84, 36–56*.

Renzullo, L. J., van Dijk, A. I. J. M., Perraud, J.-M., Collins, D., Henderson, B., Jin, H., Smith, A. B., & McJannet, D. L. (2014). Continental satellite soil moisture data assimilation improves root-zone moisture analysis for water resources assessment. *Journal of Hydrology, 519, 2747–2762*.

Romero-Trigueros, C., Nortes, P. A., Alarcón, J. J., Hunink, J. E., Parra, M., Contreras, S., Droogers, P., & Nicolás, E. (2017). Effects of saline reclaimed waters and deficit irrigation on *Citrus* physiology assessed by UAV remote sensing. *Agricultural Water Management, 183, 60–69*.

Sakai, T., Iizumi, T., Okada, M., Nishimori, M., Grünwald, T., Prueger, J., Cescatti, A., Korres, W., Schmidt, M., Carrara, A., Loubet, B., & Ceschia, E. (2016). Varying applicability of four different satellite-derived soil moisture products to global gridded crop model evaluation. *International Journal of Applied Earth Observation and Geoinformation, 48, 51–60*.

Santesteban, L. G., Di Gennaro, S. F., Herrero-Langreo, A., Miranda, C., Royo, J. B., & Matese, A. (2017). High-resolution UAV-based thermal imaging to estimate the instantaneous and seasonal variability of plant water status within a vineyard. *Agricultural Water Management, 183, 49–59*.

Schnur, M. T., Xie, H., & Wang, X. (2010). Estimating root zone soil moisture at distant sites using MODIS NDVI and EVI in a semi-arid region of southwestern USA. *Ecological Informatics, 5, 400–409*.

Su, T. C. (2017). A study of a matching pixel by pixel (MPP) algorithm to establish an empirical model of water quality mapping, as based on unmanned aerial vehicle (UAV) images. *International Journal of Applied Earth Observation and Geoinformation, 58, 213–224*.

Su, T. C., & Chou, H. T. (2015). Application of multispectral sensors carried on unmanned aerial vehicle (UAV) to trophic state mapping of small reservoirs: A case study of Tain-Pu reservoir in Kinmen, Taiwan. *Remote Sensing, 7, 10078–10097*.

Wang, X., Xie, H., Guan, H., & Zhou, X. (2007). Different responses of MODIS-derived NDVI to root-zone soil moisture in semi-arid and humid regions. *Journal of Hydrology, 340, 12–24*.

Zarco-Tejada, P. J., Diaz-Varela, R., Angileri, V., & Loudjani, P. (2014). Tree height quantification using very high resolution imagery acquired from an unmanned aerial vehicle (UAV) and automatic 3D photo-reconstruction methods. *European Journal of Agronomy, 55, 89–99*.

Contact email: spcyj@nqu.edu.tw